

Numerical simulation of unsteady galloping of two-dimensional iced transmission line with comparison to conventional quasi-steady analysis

Xiongjun Yang^a, Ying Lei^{*} and Jianguo Zhang^b

Department of Civil Engineering, Xiamen University, Xiamen 361005, China

(Received March 31, 2020, Revised April 29, 2020, Accepted May 1, 2020)

Abstract. Most of the previous works on numerical analysis of galloping of transmission lines are generally based on the quasi-steady theory. However, some wind tunnel tests of the rectangular section or hangers of suspension bridges have shown that the galloping phenomenon has a strong unsteady characteristic and the test results are quite different from the quasi-steady calculation results. Therefore, it is necessary to check the applicability of the quasi-static theory in galloping analysis of the ice-covered transmission line. Although some limited unsteady simulation researches have been conducted on the variation of parameters such as aerodynamic damping, aerodynamic coefficients with wind speed or wind attack angle, there is a need to investigate the numerical simulation of unsteady galloping of two-dimensional iced transmission line with comparison to wind tunnel test results. In this paper, it is proposed to conduct a two dimensional (2-D) unsteady numerical analysis of ice-covered transmission line galloping. First, wind tunnel tests of a typical crescent-shaped iced conductor are conducted firstly to check the subsequent quasi-steady and unsteady numerical analysis results. Then, a numerical simulation model consistent with the aeroelastic model in the wind tunnel test is established. The weak coupling methodology is used to consider the fluid-structure interaction in investigating a two-dimensional numerical simulation of unsteady galloping of the iced conductor. First, the flow field is simulated to obtain the pressure and velocity distribution of the flow field. The fluid action on the iced conductor at the coupling interface is treated as an external load to the conductor. Then, the movement of the conductor is analyzed separately. The software ANSYS FLUENT is employed and redeveloped to numerically analyze the model responses based on fluid-structure interaction theory. The numerical simulation results of unsteady galloping of the iced conductor are compared with the measured responses of wind tunnel tests and the numerical results by the conventional quasi-steady theory, respectively.

Keywords: numerical simulation; iced transmission line; galloping; unsteady analysis; quasi-steady theory; wind tunnel test

1. Introduction

The dynamic response of flexible structures such as transmission tower-line system is sensitive to wind load (Wang *et al.* 2016, Chen *et al.* 2015, 2018, Liu *et al.* 2018, Fu *et al.* 2016, Song *et al.* 2018). Iced-covered makes the transmission line asymmetric with aerodynamic instability, which easily causes the galloping of the iced transmission lines (Chen *et al.* 2018). The galloping is a self-excited vibration with low frequency and large amplitude. The safety and stability of the transmission tower-line system will be severely destroyed by the conductor galloping. Therefore, more research attention has been paid to investigate the galloping of transmission lines during the past decades (Gani *et al.* 2010, Zhou *et al.* 2015, Jia *et al.* 2019).

Generally, the numerical analysis of transmission line galloping is based on the quasi-steady theory, which assumes that the aerodynamic forces by the surrounding wind field are only related to the current relative position of

the moving structure. In other words, at every moment in the vibration, the aerodynamic force acting on the conductor section is equivalent to the static aerodynamic force under the relative wind attack angle at the moment (Dyke and Laneville 2008, Takeshi and Shinichi 2018). So, the static aerodynamic coefficient is used to calculate aerodynamic forces in the quasi-steady theory. Den Hartog (1933), Parkinson and Smith (1964), Novak (1972), Nigol and Buchan (1981a, 1981b) and other researchers have established the classical galloping theory. Then, many researchers have investigated the galloping of transmission lines based on quasi-steady theory, e.g., Ohkuma *et al.* (2000) conducted numerical analysis of transmission line galloping considering wind turbulence, Liu *et al.* (2009) studied the geometric nonlinearity of conductor motion and the eccentric inertia caused by covered ice, Lou *et al.* (2014) analyzed the effects of the ice thickness and initial angle on aerodynamic force characteristics of iced bundled conductors through wind tunnel tests, and proposed a finite element method for galloping analysis of bundled conductors, Talib *et al.* (2019) proposed a simplified dynamic model of transmission line galloping, and verified the results using experiments, Xie *et al.* (2015) and Chen *et al.* (2018) established the finite element models of the transmission tower-line system and studied the dynamic responses under wind loads, Lou *et al.* (2019) also studied

*Corresponding author, Ph.D., Professor

E-mail: ylei@xmu.edu.cn

^a M.Sc. Student

^b Ph.D., Associate Professor

the horizontal and vertical motion of the conductor and the coupling effect of different modes.

Although the quasi-steady theory has been widely used, wind tunnel aeroelastic model testing show dynamic aerodynamic force (Mannini *et al.* 2014, Cai *et al.* 2019). The influence of the conductor motion on the aerodynamic force coefficients is not considered in the quasi-steady theory, so it is not a real fluid-structure interaction study. Recently, in some wind tunnel tests of bluff bodies, such as cylinders and rectangular prisms, galloping phenomena without obvious divergent critical wind speeds have been observed, which cannot be explained by the quasi-steady mechanism. Gao and Zhu (2016, 2017) also found that the galloping phenomenon has strong unsteady characteristics through the wind tunnel test of rectangular section models, and the calculated steady-state amplitudes are quite different from the experimental results. So, they established the galloping unsteady and nonlinear self-excitation model. Chen *et al.* (2013) studied the vortex-induced vibration of stay cables and found two cable vibration behaviors: single-mode and multimode vibration. Ma *et al.* (2017) showed through wind tunnel tests of elliptical cylinders that quasi-steady theory is not suitable for predicting galloping at critical Reynolds number. Recently, Deng *et al.* (2019) conducted an unsteady theoretical study of the wake-induced vibration of hangers-on a suspension bridge.

There are very limited studies on numerical analysis of unsteady aerodynamic characteristics of iced transmission line. Zhang *et al.* (2015) analyzed the dynamic aerodynamic coefficients of the iced conductor using software FLUENT redevelopment. Lyu *et al.* (2017) carried out CFD numerical simulation of fluid-structure interaction, showing the variation rules of three degree-of-freedom (3-DOF) negative damping of conductor with wind speed and the time-frequency analysis of aerodynamic force-time history with short-time Fourier transform. These unsteady simulation researches mainly focus on the variation of parameters such as aerodynamic damping, aerodynamic coefficients with wind speed or wind attack angle. Forced harmonic vibrations with preset motions are assumed to the section of the iced lines. Therefore, there is a need for the numerical simulation study on unsteady galloping of iced transmission lines.

In this paper, it is proposed to conduct an unsteady numerical analysis of typical crescent-shaped iced transmission line galloping. Moreover, the unsteady analysis results are compared with those measured by wind tunnel tests. In the wind tunnel test, the aerodynamic forces of the iced conductor in the uniform flow field at different attack angles are measured firstly, and the instability interval of iced conductor galloping is calculated according to Den Hartog theory. Then, conductor aeroelastic model galloping tests at different wind speeds are carried out to measure the 3D displacement responses and to analyze its vibration characteristics. In terms of numerical simulation, a numerical simulation model consistent with the aeroelastic model in the wind tunnel test is established. The well-known software ANSYS FLUENT is employed to numerical analyze the model responses based on fluid-structure interaction unsteady theory. Finally, the measured responses of wind tunnel tests are compared with the

numerical simulation results based on the unsteady theory and quasi-steady theory respectively, to verify the applicability of the two theories.

2. Wind tunnel test of crescent-shaped iced conductor

2.1 Wind tunnel test of aerodynamic characteristics of iced conductor

In the conventional quasi-steady analysis of conductor galloping, the calculation of aerodynamic forces is based on the static aerodynamic force coefficients. In this paper, the typical crescent-shaped iced conductor is employed by the wind tunnel force balance test, and the variations of static aerodynamic coefficients with the wind attack angle are obtained. According to the Den Hartog destabilization criterion, the wind attack angle range prone to galloping is estimated, which provides the basis for wind tunnel test of the aeroelastic model.

2.1.1 Wind tunnel test model and equipment

The iced conductor model is made of fiber-reinforced plastics (FRP) and its section is shown in Fig.1. The conductor is modeled by the common type LGJ-400/35 with 13.4mm in radius. The model section is composed of half circle and half ellipse, the short half axis of the ellipse is 13.4mm and the long one is 33.5mm. The length of the model is 1m.

The test was carried out in the wind tunnel laboratory of Xiamen University of Technology. The length, width and height of the wind tunnel are 8m, 2.6m and 2.8m, respectively, and the flow field in the test section is of high quality and the maximum design wind speed is 90m/s. This section model test was conducted in a uniform flow field with a wind speed of 10m/s. The force measuring equipment was the six-component force balance of SI-130-10. The sampling time was 30s with 200Hz sampling frequency. The test model and equipment are shown in Fig.1.

2.1.2 The testing results

The lifting and drag forces and moment on the conductor model are dimensionless, and the aerodynamic force coefficients are estimated by (Keutgen and Lilien 2000)

$$C_L = \frac{F_L}{0.5\rho U^2 Ld}, \quad C_D = \frac{F_D}{0.5\rho U^2 Ld}, \quad C_M = \frac{F_M}{0.5\rho U^2 Ld^2} \quad (1)$$

where C_L, C_D, C_M are the coefficients of lifting, drag and moment respectively, U is the wind speed, ρ is the air density, L is the effective length, d is the diameter of the conductor model.

The variations of the above aerodynamic coefficients with wind attack angle can be obtained by Eq.(1), and the results are shown in Fig.2.

According to the Den Hartog instability criteria (Den. Hartog, 1933), the damping term is negative when the conductor is galloping, one can obtain as:

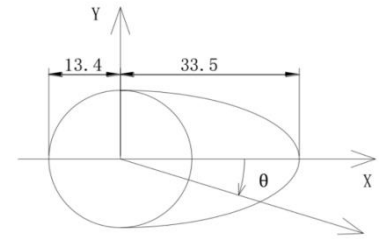
$$\delta = \frac{\partial C_L}{\partial \theta} + C_D < 0 \quad (2)$$



(a) Test model and equipment



(b) Model section



(c) Model section

Fig. 1 The test model and equipment

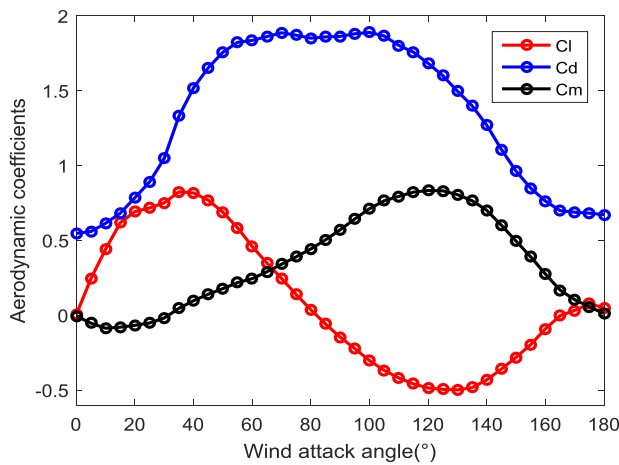


Fig. 2 The aerodynamic coefficients

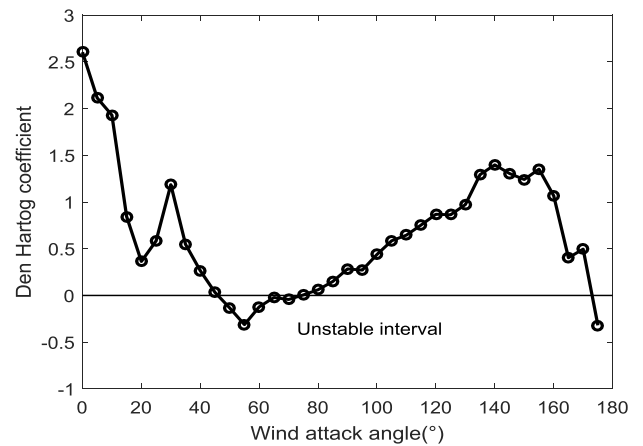


Fig. 3 Den Hartog stability coefficient

in which, δ is Den Hartog coefficient. When $\delta < 0$, the conductor undergoes vertical galloping if the wind speed reaches maximum. By inserting the obtained aerodynamic force coefficients into Eq. (2), the wind attack angle range which is prone to aerodynamic instability is obtained. As seen in Fig. 3, when the wind attack angle is about $50^\circ \sim 65^\circ$ or near 175° , Den Hartog coefficient is $\delta < 0$.

2.2 Wind tunnel test of aeroelastic model

A 3-DOF iced conductor aeroelastic model with the same section in Sect. 2.1.1 has been performed to compare with subsequent quasi-steady and unsteady numerical analysis results. The vibration displacements of the model were recorded by laser displacement meters.

2.2.1 Test model and equipment

As shown in Fig. 4, an aeroelastic model of iced conductor with 3-DOFs of vertical- horizontal-twist was tested in the wind tunnel. The model was fixed at the center of the two lifting arms, one of which was suspended on the fixed outer bracket by six springs. The vertical and horizontal stiffness of the model could be provided by the vertical and horizontal springs, and the torsional stiffness could be controlled by the vertical spring stiffness and the distance between the spring suspension points and the lifting arm centers. The moment of inertia of the model was

Table 1 The parameters of the model

Total model mass (kg)	31.9
Total stiffness of upper spring (N/m)	4×400
Total stiffness of the lower spring (N/m)	4×196
Total stiffness of transverse spring (N/m)	4×196
Vertical spring spacing (m)	0.5
The length of lifting arm (m)	1.0
The weight at both ends of lifting arms (kg)	4×0.66

provided by the lifting arms and the weight fixed on both ends of the arms. The parameters of the model are listed in Table. 1.

As shown in Fig. 5, two vertical laser meters were fixed on both sides of the lifting arms and the distances between the two lasers and the origin were both d_1 . A beam of transverse laser with distance d_2 above the origin reflected from the plate fixed vertically on the model.

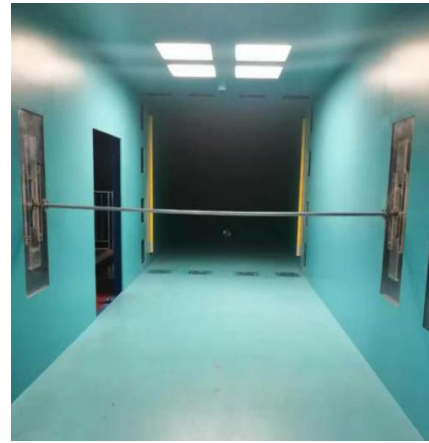
Based on geometry in Fig.5, it is known that

$$\theta = \arctan\left(\frac{\bar{y}_2 - \bar{y}_1}{2d_1}\right) ; \tag{3}$$

$$x = \bar{x} + (d_2 - y) \tan \theta ; y = \bar{y}_1 + (x + d_1) \tan \theta$$



(a) External diagram of test model



(b) Internal diagram of test model

Fig. 4 The aeroelastic model in wind tunnel test

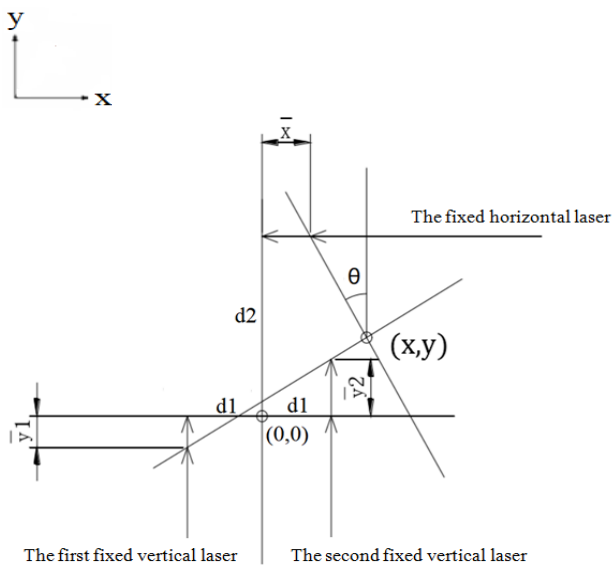


Fig. 5 The measurement by laser displacement meter

where \bar{y}_1 , \bar{y}_2 and \bar{x} denote the measurements of the first, second vertical laser and the transverse laser, respectively. θ , x and y are the torsion angle, horizontal and vertical displacements of the model, which can be obtained by solving Eq. (3).

2.2.2 Calibration of model vibration frequencies and damping ratios

To save page space, only the time history of vertical free attenuation displacement of the model and the spectrum analysis results of the 3-DOF free attenuation motion are shown in Fig. 6.

The model vibration frequencies and damping ratios need to be calibrated through the free attenuation motions. The vertical, horizontal and torsional natural frequencies are identified as 1.43Hz, 1.31Hz and 2.32Hz with the corresponding damping ratio of 0.098%, 0.1% and 0.5%.

2.2.3 The testing results

In the wind tunnel test of the aeroelastic model, the wind speed of the uniform flow field was increased from 6m/s to

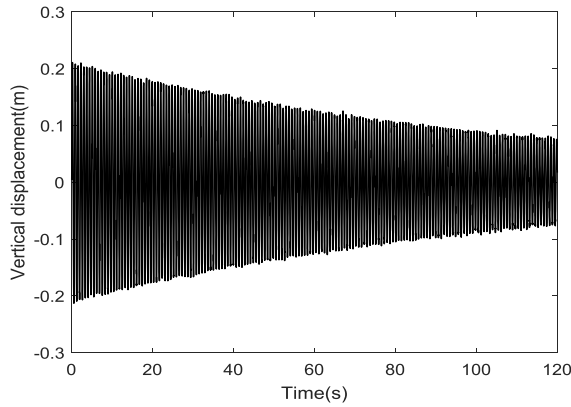
11.5m/s gradually at 0.5m/s intervals. From the results in Sect. 2.1.2, it was found that with the wind attack angles of 180° , the conductor galloping may occur. Fig. 7 shows the variations of vibration amplitudes with the wind speed. When the wind speed is less than 10m/s, there was no conductor galloping, but galloping occurred in the vertical movement when the wind speed reached around 10.5m/s.

3. Numerical simulation for unsteady galloping of aeroelastic model

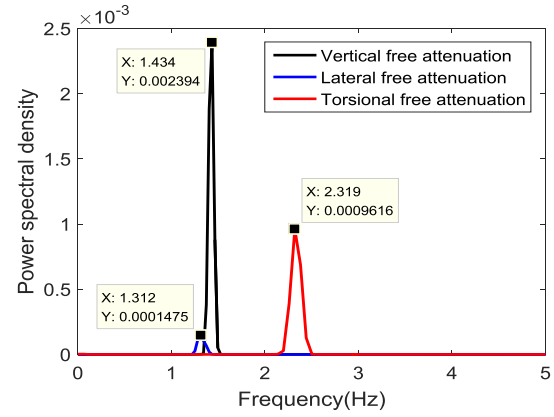
A numerical simulation model consistent with the aeroelastic model in the wind tunnel test is established. The numerical simulation of unsteady conductor galloping belongs to the bi-directional fluid-structure interaction problem. The numerical solution of fluid-structure interaction can generally be divided into the strong coupling method and the weak coupling method. The strong coupling method is to put the structure domain, fluid domain and coupling effect into the same set of control equations and solve all variables simultaneously. This method has higher accuracy, but its calculation process is extremely complicated. In the weak coupling methodology, the fluid dynamic equation and structural dynamic equation are solved subsequently, and the computational data in the fluid domain and vibration variables in the structure domain are exchanged through the fluid-structure interaction interface. The weak-coupling method has been widely used because of its applicability and easy solution compared with the strong-coupling method. Hence, the weak coupling methodology is adopted herein to consider the fluid-structure interaction effect in investigating the dynamic aerodynamic characteristics of the iced conductor in the process of relative movement between the ice-covered conductors (Takeshi and Shinichi 2018). In this paper, the software ANSYS FLUENT is employed for numerical analysis of the model unsteady galloping.

3.1 The numerical simulation of the flow field

First, the numerical simulation of the 2-D flow field



(a) Vertical free attenuation displacement



(b) Spectrum of free attenuation motion

Fig. 6 The free attenuation displacement and the spectra

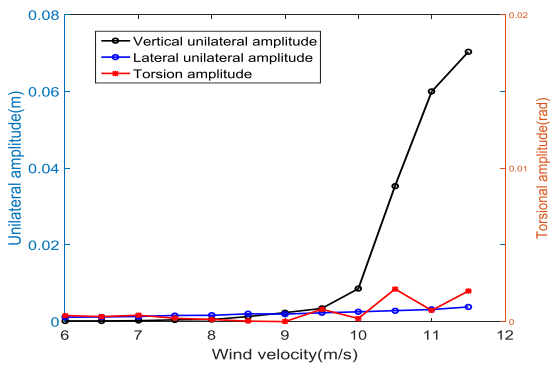


Fig. 7 Variations of displacement amplitudes with wind speed

around the crescent-shaped iced conductor is discussed in this section.

3.1.1 Governing equations

The governing equation of the flow field can be described by 2D incompressible viscous fluid mass conservation equations and momentum conservation equations. The mass conservation equation is a mathematical description of the law of mass conservation. The law of conservation of mass is expressed as the increase of mass in a fluid microelement per unit time equal to the net mass flowing into the microelement at the same time interval. According to this expression, the mass conservation equation can be obtained (Shao *et al.* 2003):

$$\frac{\partial u}{\partial x} + \frac{\partial v}{\partial y} = 0 \quad (4)$$

u and v are the velocity of the fluid in the x and y directions, respectively.

The momentum conservation equation is a mathematical description of the law of momentum conservation. The law of momentum conservation is expressed as follows: the rate of change of fluid momentum in a microcellular body to time is equal to the sum of all forces acting on the microcellular body by external forces. The law of conservation of momentum is essentially Newton's second law. According to this law, the momentum conservation equation i.e., Navier-Stokes (N-S) equation of the fluid

microelement is obtained as follows (Shao *et al.* 2003):

$$\left. \begin{aligned} \frac{\partial u}{\partial t} + u \frac{\partial u}{\partial x} + v \frac{\partial u}{\partial y} &= \frac{\mu}{\rho} \left(\frac{\partial^2 u}{\partial x^2} + \frac{\partial^2 u}{\partial y^2} \right) - \frac{1}{\rho} \frac{\partial p}{\partial x} \\ \frac{\partial v}{\partial t} + u \frac{\partial v}{\partial x} + v \frac{\partial v}{\partial y} &= \frac{\mu}{\rho} \left(\frac{\partial^2 v}{\partial x^2} + \frac{\partial^2 v}{\partial y^2} \right) - \frac{1}{\rho} \frac{\partial p}{\partial y} \end{aligned} \right\} \quad (5)$$

where ρ is fluid density, μ is coefficient of kinetic viscosity, p is flow pressure.

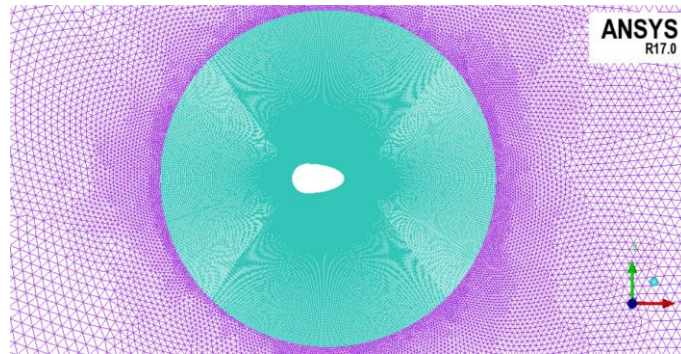
Moreover, turbulence flow should be considered in the flow around the iced conduct. Herein, Reynolds Averaged Navier-Stokes (RANS) method with the standard SST (shear stress transport) k - ω turbulence model is employed as its calculation accuracy in the flow around blunt body is relatively high. SST k - ω model is the eddy-viscosity model which combines the advantages of the k - ω and k - ϵ models. The k - ω model is used in the near-wall region, and the k - ϵ model is used in region away from wall (Zhang *et al.* 2015). The transport equation in the k - ϵ model is:

$$\begin{aligned} \frac{\partial(\rho k)}{\partial t} + \frac{\partial(\rho k u)}{\partial x} &= \frac{\partial}{\partial x} \left[\left(\mu + \frac{\mu_t}{\sigma_k} \right) \frac{\partial k}{\partial x} \right] + G_k - \rho \epsilon \\ \frac{\partial(\rho \epsilon)}{\partial t} + \frac{\partial(\rho \epsilon u)}{\partial x} &= \frac{\partial}{\partial x} \left[\left(\mu + \frac{\mu_t}{\sigma_\epsilon} \right) \frac{\partial \epsilon}{\partial x} \right] \\ &\quad + \frac{\epsilon}{k} (C_{1\epsilon} G_k - C_{2\epsilon} \rho \epsilon) \end{aligned} \quad (6)$$

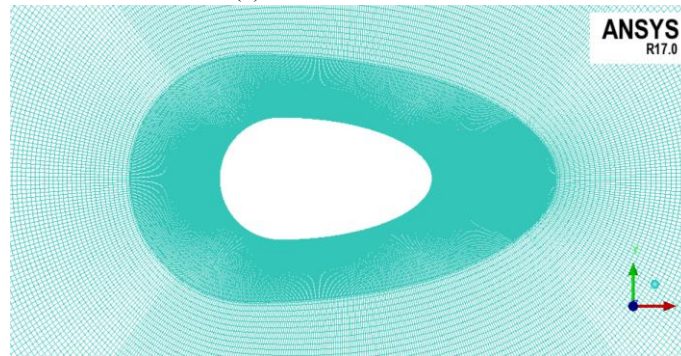
in which, k is the kinetic energy of the turbulence, ϵ is the dissipation rate of the turbulent kinetic energy, σ_k and σ_ϵ are the Prandtl numbers corresponding to the turbulent energy and dissipation rate, respectively, $C_{1\epsilon}$, $C_{2\epsilon}$ and C_μ are model constants, respectively, and $u_t = \rho C_\mu k^2 / \epsilon$. G_k is the turbulent kinetic energy caused by the average velocity.

3.1.2 Numerical solution

To numerically solve the complex partial differential equations describing fluid flow, Eqs. (4)-(5), the computational region needs to be discretized in order to discretize these partial differential equations. The finite volume method (FVM), one of the commonly used discretization method in CFD, is adopted in this paper, it divides the whole computational domain into finite mesh



(a) Mesh of flow field



(b) Mesh of near-wall region

Fig. 8 Mesh of the flow field

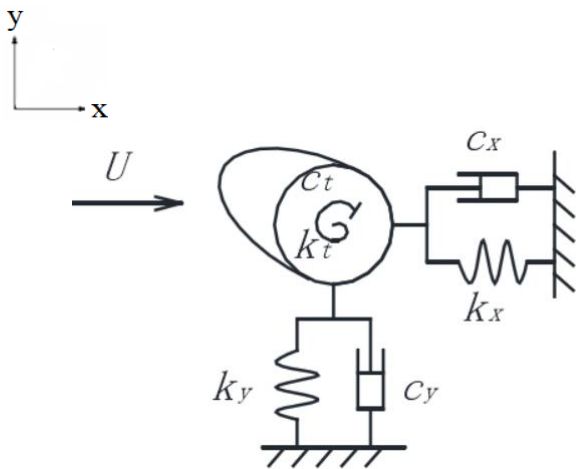


Fig. 9 Dynamic model of the iced conductor

and has a non-overlapping micro-body around each mesh node. By dividing the control equation into each micro-element volume, a set of discretized equations is obtained.

First, an appropriate calculation domain should be selected, which can not only shorten the calculation time but also reduce the influence of the boundary on the calculation of the flow field. Herein, the size of the computational field is estimated by the idea of blocking rates (Lyu *et al.* 2017). Based on the geometric size of the model, the flow field is selected as a rectangular region with a length of 1.6m and a width of 1.2m. The left side is the velocity inlet while the right side is the pressure outlet, and the upper and lower bounds are symmetric rigid boundaries.

The surface of the iced conductor is set as no sliding wall. The incoming wind speed is taken as the uniform flow

of 6m/s-11.5m/s corresponding to the wind tunnel test. Based on the wind tunnel testing results in Sect. 2.1.2, the initial wind attack angle is selected as 180°.

To improve the computational efficiency, dynamic grid updating with the combination of mesh adjustment based on elastic deformation and local grid refinement is adopted. The unstructured collocated mesh is used to divide the non-near-wall region, and a refined structured mesh is used for the near-wall region. The dynamic mesh is generated using the Remeshing method build-in FLUENT. The maximum size of the local mesh is 3mm and the minimum size is 2mm. The mesh division of calculation domain is as shown in figure 8.

In this paper, the semi-implicit method for pressure linked equation (SIMPLE) algorithm is employed for solving the discretized equations. The SIMPLE algorithm is based on pressure correction approach, in which pressure field and velocity field are calculated iteratively (Zhang *et al.*, 2015). With the given pressure field, the discrete N-S equation is first solved to obtain the velocity field. Then, the relationship between pressure and velocity is inserted into the discrete- continuous equation to obtain the corrected pressure. Then, a new velocity field is obtained by corrected pressure field. The velocity field is checked for convergence, and the iteration is started until a convergent solution is obtained.

3.2 The numerical simulation of the iced conduct vibration

The software FLUENT can only calculate the flow field motion. Redevelopment of FLUENT with the tool of User

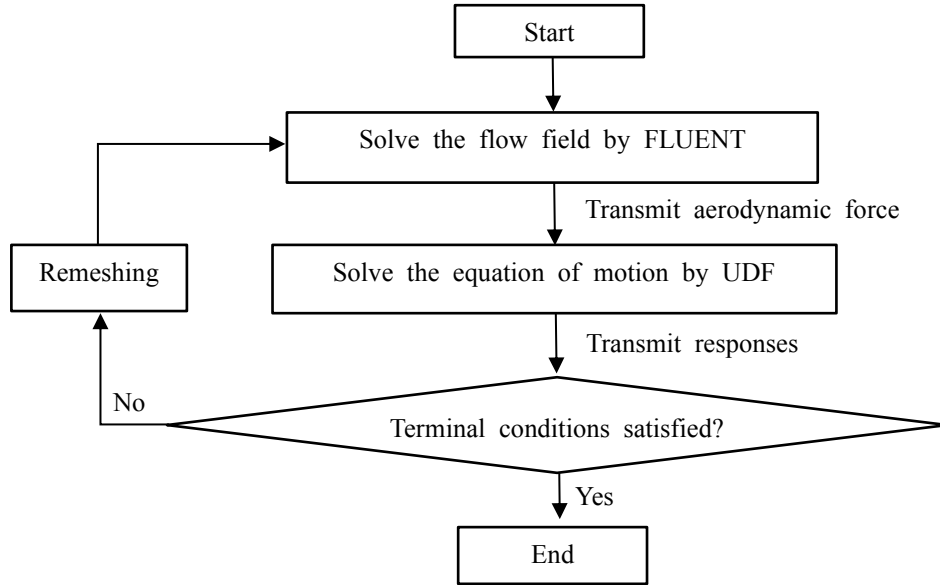


Fig. 10 Flow chart of numerical unsteady analysis of conduct galloping

Defined Function (UDF) in ANSYS, which is a programming interface that extends the specific functions of FLUENT with C language, is employed for the numerical solution of the iced conduct vibration under the flow motion.

A numerical model consistent with the wind tunnel aeroelastic model in Sect. 2.2 is established. Since the shape and motion state of each section of the aeroelastic model are identical, the numerical model can be simplified as a plane 3-DOF motion model as shown in Fig. 9.

The motion equation of the conductor model can be expressed as:

$$\begin{bmatrix} m & 0 & S_y \\ 0 & m & S_x \\ S_y & S_x & J \end{bmatrix} \begin{Bmatrix} \ddot{y} \\ \ddot{x} \\ \ddot{\theta} \end{Bmatrix} + \begin{bmatrix} c_y & 0 & 0 \\ 0 & c_x & 0 \\ 0 & 0 & c_\theta \end{bmatrix} \begin{Bmatrix} \dot{y} \\ \dot{x} \\ \dot{\theta} \end{Bmatrix} + \begin{bmatrix} k_y & 0 & 0 \\ 0 & k_x & 0 \\ 0 & 0 & k_\theta \end{bmatrix} \begin{Bmatrix} y \\ x \\ \theta \end{Bmatrix} = \begin{Bmatrix} F_y \\ F_x \\ F_\theta \end{Bmatrix} \quad (7)$$

where m is unit length mass of conductor, S_y and S_x are unit length mass moment about y -axis and x -axis, respectively, J is unit length moment of inertia. c_y, c_x, c_θ and k_y, k_x, k_θ are unit length damping and stiffness in vertical, horizontal, and torsional directions, respectively. The damping and stiffness values are obtained from the wind tunnel test in Sect. 2.2, and F_y, F_x, F_θ are unit length aerodynamic forces from the flow field in three directions. In this paper, the Newmark- β method is used for the numerical solution of Eq. (7) under the aerodynamic forces from the numerical simulation results of the fluid field.

3.3 Weak coupling approach for unsteady numerical analysis of conduct galloping

In this paper, DEFINE_CG_MOTION macro in ANSYS FLUENT is adopted in the fluid-structure interaction simulation to realize the coordinate movement of iced conductor gravity centre, the calculation of the conductor vibration and the calculation data exchange. In each calculation step, the flow field is first solved to estimate the

intensity of pressure on the conductor wall and the results are transferred to UDF. The pressure obtained through integration on the wall surface of the conductor in UDF is translated into the three aerodynamic forces on the conduct motion equation, Eq.(7). Then, the structural response is calculated and the movement information is transmitted to FLUENT, which moves the model to the corresponding location and the flow mesh is updated. It is worth noting that the aerodynamic forces are obtained by solving the governing equation of the fluid domain by FLUENT in the unsteady numerical simulation instead of using the aerodynamic coefficients in the quasi-steady analysis. The flow chart of the unsteady numerical analysis of conduct galloping is summarized in Fig.10.

3.4 Results of unsteady galloping with comparisons to those by experiment and quasi-steady analysis

Fig. 11 shows the velocity cloud diagram of the flow field at different time when the wind speed is 11m/s. It is clear that there is a static wind zone at the stagnation point on the top of the conductor, the wind speed reaches the maximum at the separation points of the flow field on both sides of the conductor, the flow field is obvious symmetric, and the wind speed is small in the wake area and the vortex shedding occurs

In the quasi-steady analysis, the aerodynamic forces are estimated based on the quasi-steady theory, which assumes that the aerodynamic forces are the static aerodynamic forces under the relative wind attack angle, i.e.,

$$\{F_y \ F_x \ F_\theta\}^T = 0.5\rho U^2 d \{C_y(\alpha) \ C_x(\alpha) \ dC_M(\alpha)\}^T \quad (8)$$

$$C_y(\alpha) = C_L(\alpha)\cos(\Delta\theta) - C_D(\alpha)\sin(\Delta\theta) \quad (9a)$$

$$C_x(\alpha) = C_L(\alpha)\sin(\Delta\theta) + C_D(\alpha)\cos(\Delta\theta) \quad (9b)$$

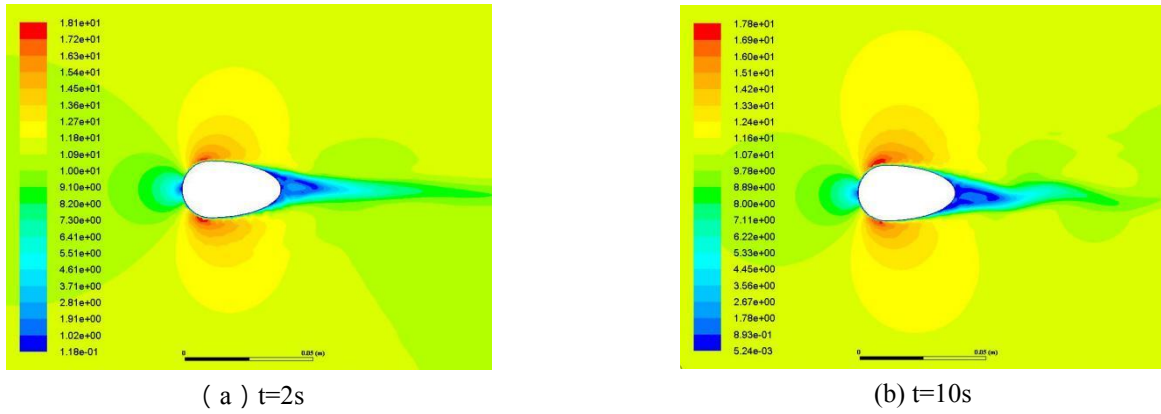


Fig. 11 Velocity cloud at different times in unsteady analysis

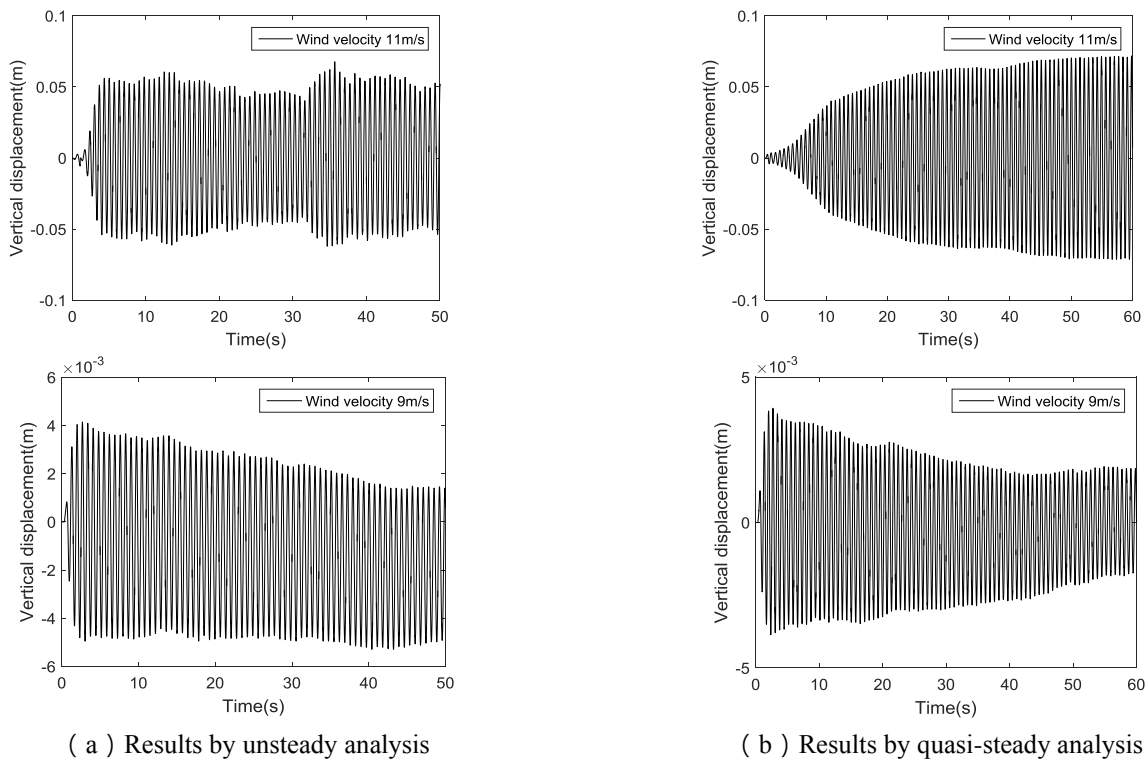


Fig. 12 Time history of vertical displacement

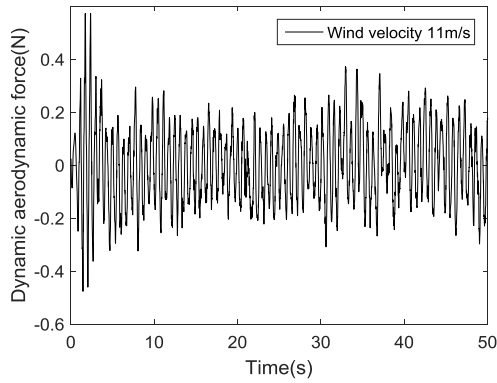
where α is relative wind attack angle, $\alpha = \alpha_0 + \theta - \Delta\theta$, α_0 is initial wind attack angle and is consistent with the one of wind tunnel test 180° . θ is rotation angle of the conductor model, $\Delta\theta$ is the change of wind attack angle due to the movement of conduct model, $\Delta\theta = \left(\frac{\dot{y}}{U} + \frac{R\dot{\theta}}{U}\right)$, R is conductor radius and U is the wind speed in the wind tunnel test.

Fig. 12 shows the vertical displacements of the iced conductor by the unsteady and quasi-steady analysis respectively. When the wind speed is 9m/s, the displacement first increases and then converges. When the wind speed is 11m/s, the displacement first diverges and then gradually tends to be stable. The vibration amplitudes and trends by the two analyses are similar.

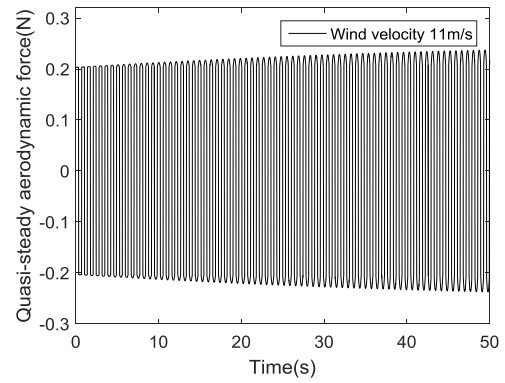
Fig. 13 compares the vertical aerodynamic forces by the unsteady and quasi-steady simulation with wind speed of

11m/s. The time histories of two kinds of aerodynamic forces are quite different.

Finally, Fig. 14 compares the variation of vertical vibration amplitudes at different wind speeds by unsteady and quasi-stationary calculation results. The numerical calculation results are also compared with the wind tunnel results. Generally, the differences between the unsteady and quasi-steady results are small, the critical wind speeds by the two analyses are around 10.5m/s, which are consistent with the wind tunnel test results, and the vibration amplitude and growth trend are basically the same as the test. According to the defined error by Eq. (10), the maximum error and average error of quasi-steady calculation results are 40.25% and 25.58%, while the maximum error and average error of unsteady results are 19.94% and 15.74% respectively.



(a) Dynamic aerodynamic forces



(b) Quasi-steady aerodynamic forces

Fig. 13 Comparisons of aerodynamic forces by unsteady and quasi-steady analysis

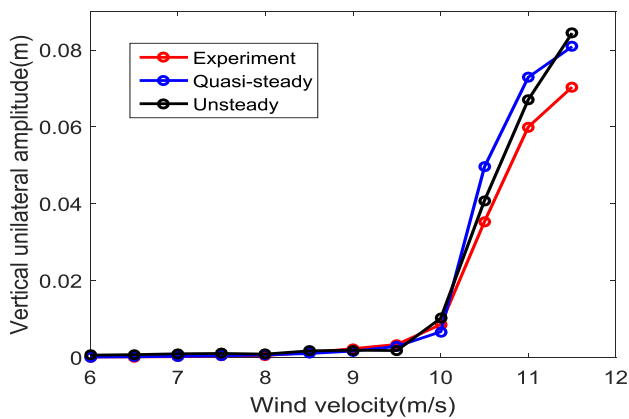


Fig. 14 Comparison of unsteady and quasi-stationary galloping by numerical and test analyses

$$\varepsilon = \frac{|A_c - A_m|}{A_m} \quad (10)$$

where ε is error, A_c is calculated amplitude by numerical simulation and A_m is measured amplitude in the wind tunnel test.

4. Conclusions

Numerical analysis of iced transmission line galloping based on quasi-steady approach has been widely used, but this is not a complete fluid-structure interaction analysis in real sense so this quasi-steady theory still needs to be checked. Although limited studies have been conducted on numerical analysis of unsteady aerodynamic characteristics of iced transmission lines, forced harmonic vibrations with preset motions are assumed to the iced conduct model. Therefore, there is a need for the numerical simulation study on unsteady galloping of iced transmission lines that the results could be compared to wind tunnel tests and quasi-steady approach results. In this paper, numerical simulation of 2D crescent-shaped iced transmission line galloping has been implemented based on the weak coupling methodology. The fluid dynamic equation and structural dynamic equation are solved subsequently, and

the computational results in the fluid domain and vibration state in the structure domain are exchanged through the fluid-structure interaction interface. The aerodynamic force is obtained by solving the governing equation of the fluid domain in the unsteady numerical simulation instead of using the aerodynamic force coefficients in the quasi-steady analysis. All numerical simulations are implemented by the software ANSYS FLUENT and the redevelopment with the tool of User Defined Function (UDF). Wind tunnel test of the same crescent-shaped iced conduct model has validated the proposed numerical simulation results of unsteady galloping. Moreover, the quasi-steady numerical simulation is also conducted to compare with the unsteady analysis and the wind tunnel experimental test. In general, the vibration amplitudes under different wind speeds calculated by the unsteady and quasi-steady numerical analysis are similar, and the quasi-steady analysis could reflect the variation trend of transmission line galloping. However, the time histories of the vibration response calculated by the quasi-steady analysis are different from those by the unsteady analysis, so it is preferred to implement unsteady analysis for iced conductor galloping. Also, the time histories of the aerodynamic force calculated by the unsteady analysis are different from those by the quasi-steady analysis. The unsteady aerodynamic force is calculated by considering the real fluid-structure interaction, but the quasi-steady aerodynamic force is estimated using the static aerodynamic coefficients.

Acknowledgments

This research is financially supported by the National Key R&D Program of China through the Grant No. 2017YFC0803300. The authors also thank the supports from the wind tunnel laboratory of Xiamen University of Technology for conducting the wind tunnel test in this paper.

References

Cai, M., Zhou, L., Lei, H. and Huang, H. (2019), "Wind tunnel test Investigation on unsteady aerodynamic coefficients of iced 4-bundle conductors", *Adv. Civil Eng.*, **2019**, 1-12.

- <https://doi.org/10.1155/2019/2586242>.
- Chen, B., Wu, J.B., Ouyang, Y. and Deng, Y. (2018), "Response evaluation and vibration control of a transmission tower-line system in mountain areas subjected to cable rupture", *Struct. Monitor. Maintenance*, **5**(1), 151-171. <https://doi.org/10.12989/smm.2018.5.1.151>.
- Chen, B., Xiao, X., Li, P.Y. and Zhong, W.L. (2015), "Performance evaluation on transmission tower-line system with passive friction dampers subjected to wind excitations", *Shock Vib.*, **2015**(2015), 1-13. <https://doi.org/10.1155/2015/310458>.
- Chen, W. L., Li, H., Ou, J.P. and Li, F. (2013), "Numerical simulation of vortex-induced vibrations of inclined cables under different wind profiles", *J. Bridge Eng.*, **18**(1), 42-53. [http://dx.doi.org/10.1061/\(ASCE\)BE.1943-5592.0000323](http://dx.doi.org/10.1061/(ASCE)BE.1943-5592.0000323)
- Deng, Y.C., Li, S.Y. and Chen, Z.Q. (2019), "Unsteady theoretical analysis on the wake-induced vibration of suspension bridge hangers", *J. Bridge Eng.*, **24**(2), 04018113. [http://dx.doi.org/10.1061/\(ASCE\)BE.1943-5592.0001339](http://dx.doi.org/10.1061/(ASCE)BE.1943-5592.0001339)
- Dyke, P. V. and André, L. (2008), "Galloping of a single conductor covered with a d-section on a high-voltage overhead test line", *J. Wind Eng. Ind. Aerodyn.*, **96**(6-7), 1141-1151. <https://doi.org/10.1016/j.jweia.2007.06.036>.
- Fu, X. and Li, H.N. (2016), "Dynamic analysis of transmission tower-line system subjected to wind and rain loads", *J. Wind Eng. Ind. Aerodyn.*, **157**, 95-103. <https://doi.org/10.1016/j.jweia.2016.08.010>.
- Gani, F. and Legeron, F. (2010), "Dynamic response of transmission lines guyed towers under wind loading", *Can J. Civil Eng.*, **37**(3), 450-465. <https://doi.org/10.1139/L09-160>.
- Gao, G. Z. and Zhu, L.D. (2016), "Measurement and verification of unsteady galloping force on a rectangular 2:1 cylinder", *J. Wind Eng. Ind. Aerodyn.*, **157**, 76-94. <https://doi.org/10.1016/j.jweia.2016.08.004>.
- Gao, G. Z. and Zhu, L.D. (2017), "Nonlinear mathematical model of unsteady galloping force on a rectangular 2:1 cylinder", *J. Fluid Struct.*, **70**, 47-71. <https://doi.org/10.1016/j.jfluidstructs.2017.01.013>.
- Hartog, J. P. D. (1933), "Transmission line vibration due to sleet", *Transactions of the American Institute of Electrical Engineers*, **51**(4), 1074-1076. <https://doi.org/10.1109/T-AIEE.1932.5056223>.
- Jia, X.L., Fu, X., and Li, H.N. (2019), "Experimental study on aerodynamic characteristics of conductors covered with crescent-shaped ice", *Wind Struct.*, **29**(4), 225-234. <https://doi.org/10.12989/was.2019.29.4.225>.
- Keutgen, R., and Lilien, J. L. (2000), "Benchmark cases for galloping with results obtained from wind tunnel facilities validation of a finite element model", *IEEE Transactions on Power Delivery*, **15**(1), 367-374. <https://doi.org/10.1109/61.847275>.
- Liu, Z.J., Liu, Z.H. and Peng, Y.B. (2018), "Simulation of multivariate stationary stochastic processes using dimension-reduction representation methods", *J. Sound Vib.*, **418**, 144-162. <https://doi.org/10.1016/j.jsv.2017.12.029>.
- Liu, X.H., Yan, B., Zhang, H.Z. and Zhou, S. (2009), "Nonlinear numerical simulation method for galloping of iced conductor", *Appl. Math. Mech.*, **30**(04), 89-101. <https://doi.org/10.1007/s10483-009-0409-x>.
- Lou, W. J., Wu, D.G. and Xu, H.W. (2019), "Wind-induced conductor response considering the nonproportionality of generalized aerodynamic damping", *J. Mech. Sci. Technol.*, **33**(1). <https://doi.org/10.1007/s12206-019-0602-9>.
- Lou, W.J., Yang, L., Lv, J. and Huang, M.F. (2014), "Aerodynamic force characteristics and galloping analysis of iced bundled conductors", *Wind Struct.*, **18**(2), 135-154. <https://doi.org/10.12989/was.2014.18.2.135>.
- Liu, Z.B., Chen, W.L., Pan, Y., Zhang, B. and Li, Q. (2017), "Numerical simulation on galloping of an iced conductor", *J. Natural Disasters*, **26**(4), 1-9. <https://doi.org/10.13577/j.jnd.2017.0401>.
- Ma, W.Y., Macdonald, J.H.G., Liu, Q., Nguyen, C.H. and Liu, X.B. (2017), "Galloping of an elliptical cylinder at the critical Reynolds number and its quasi-steady prediction", *J. Wind Eng. Ind. Aerodyn.*, **168**, 110-122. <https://doi.org/10.1016/j.jweia.2017.04.022>.
- Mannini, C., Marra, A.M. and Bartoli, G. (2014), "Viv-galloping instability of rectangular cylinders: review and new experiments", *J. Wind Eng. Ind. Aerodyn.*, **132**, 109-124. <https://doi.org/10.1016/j.jweia.2014.06.021>.
- Nigol, O. and Buchan, P.G. (1981), "Conductor galloping part I-Den Hartog mechanism", *IEEE Transactions on Power Apparatus Syst.*, **PAS-100**(2), 699-707. <https://doi.org/10.1109/TPAS.1981.316921>.
- Nigol, O. and Buchan, P.G. (1981), "Conductor galloping-part II torsional mechanism", *IEEE Transactions on Power Apparatus Syst.*, **PAS-100**(2), 708-720. <https://doi.org/10.1109/TPAS.1981.316922>.
- Novak, M. (1972), "Galloping oscillations of prismatic structures", *J. Eng. Mech.*, **98**(1), 27-46. <http://worldcat.org/issn/07339399>.
- Ohkuma, T., Kagami, J., Nakauchi, H., Kikuchi, T. and Marukawa, H. (2000), "Numerical analysis of overhead transmission line galloping considering wind turbulence", *Electr. Eng. Jpn.*, **131**(3), 19-33. [https://doi.org/10.1002/\(SICI\)1520-6416\(200003\)131:3<19::AID-EEJ3>3.0.CO;2-S](https://doi.org/10.1002/(SICI)1520-6416(200003)131:3<19::AID-EEJ3>3.0.CO;2-S).
- Parkinson, G.V., J.D. Smith, J.D. (1964), "The square prism as an aeroelastic nonlinear oscillator", *J. Mech Appl Math.*, **17**, 225-239. <https://doi.org/10.1093/qjmam/17.2.225>.
- Song, Y.P., Chen, J.B., Peng, Y.B., Spanos, P.D. and Li, J. (2018), "Simulation of nonhomogeneous fluctuating wind speed field in two-spatial dimensions via an evolutionary wavenumber-frequency joint power spectrum", *J. Wind Eng. Ind. Aerodyn.*, **179**, 250-259. <https://doi.org/10.1016/j.jweia.2018.06.005>.
- Shao, S.D. and Lo, E.Y. M. (2003), "Incompressible SPH method for simulating Newtonian and non-Newtonian flows with a free surface", *Adv. Water Res.*, **26**(7), 787-800. [https://doi.org/10.1016/S0309-1708\(03\)00030-7](https://doi.org/10.1016/S0309-1708(03)00030-7).
- Takeshi, I. and Shinichi, O. (2018), "A numerical study of the aerodynamic characteristics of ice-accreted transmission lines", *J. Wind Eng. Ind. Aerodyn.*, **177**, 60-68. <https://doi.org/10.1016/j.jweia.2018.04.008>.
- Talib, E., Shin, J., Kwak, M. K. and Koo, J.R. (2019), "Dynamic modeling and simulation for transmission line galloping", *J. Mech Sci Technol*, **33**(9), 4173-4181. <https://doi.org/10.1007/s12206-019-0812-1>
- Wang, H., Tao, T.Y., Li, A. and Zhang, Y. (2016), "Structural health monitoring system for Sutong cable-stayed bridge", *Smart Struct. Syst.*, **18**(2), 317-334. <https://doi.org/10.12989/sss.2016.18.2.317>.
- Xie, W.P., Chen, B., Li, P.Y. and Gong, X.F. (2015), "Research on dynamic responses of a transmission tower under monsoon wind", *App. Mech. Mater.*, **744-746**, 248-252. <https://doi.org/10.4028/www.scientific.net/AMM.744-746.248>.
- Zhang, Z., Yang, X.P. and Hao, S.Y. (2015), "Numerical simulation and analysis of dynamic aerodynamic characteristics of iced conductor". *J. Vib. Shock*, **34**(7), 209-214 (in Chinese). <http://jvs.sjtu.edu.cn/CN/Y2015/V34/I7/209>.
- Zhou, L., Yan, B., Zhang, L. and Zhou, S. (2015), "Study on galloping behavior of iced eight bundle conductor transmission lines", *J. Sound Vib.*, **362**, 85-110. <https://doi.org/10.1016/j.jsv.2015.09.046>.